Optics Letters

Fabrication of controllably variable sub-100 nm gaps in silver nanowires by photothermal-induced stress

Pintu Ghosh,[1] Jinsheng Lu,[1] Hao Luo,[1] Ziquan Xu,[1] Xiaoyuan Yan,[2] Yewu Wang,[2] Jun Lu,[1] Min Qiu,[1] and Qiang Li[1,*]

[1]State Key Laboratory of Modern Optical Instrumentation, College of Optical Science and Engineering, Zhejiang University, Hangzhou 310027, China
[2]Department of Physics & State Key Laboratory of Silicon Materials, Zhejiang University, Hangzhou 310027, China
*Corresponding author: qiangli@zju.edu.cn

Received 19 February 2018; revised 22 March 2018; accepted 24 March 2018; posted 28 March 2018 (Doc. ID 323465); published 15 May 2018

A technique to fabricate nanogaps with controllably variable gap width in silver (Ag) nanowires (NWs) by photothermal-induced stress utilizing a focused continuous-wave laser (532 nm) is presented. For the case of an Ag NW on gold thin film, a gap width starting from ~20 nm is achieved with a critical minimum power (CMP) of about 160 mW, whereas in the case of an Ag NW placed on top of a zinc oxide NW, the attained gap width is as small as a few nm (<10 nm) with a CMP of only ~100 mW. In both cases, the CMP is much lower as compared to the required CMP (~280 mW) for an Ag NW placed on a bare silica substrate. The photothermal-induced stress combined with Rayleigh instability, melting, and sublimation of Ag aids in breaking the Ag NW. In particular, the former one plays a key role in attaining an extremely narrow gap. This technique to fabricate sub-100 nm nanogaps in metal NWs can be extensively implemented in fabrication and maintenance of nanomechanical, nanoplasmonic, and nanoelectronic devices.

OCIS codes: (220.4241) Nanostructure fabrication; (350.5340) Photothermal effects; (240.6680) Surface plasmons.

https://doi.org/10.1364/OL.43.002422

Recent advances in synthesis of metal nanowires (NWs) have opened up new avenues for their application in diverse fields of nanoscience and nanotechnology, including nanoelectronics [1], nanophotonics [2], nanomedicine [3], and nanomechanical systems [4]. In this regard, silver (Ag) NW is one of the most commonly used ones due to the ease of fabrication and its broad range of applicability, such as transparent conducting electrodes [5], flexible displays [6], and solar cells [7]. Towards utilizing the Ag NWs for the above-mentioned applications, the most basic requirements are the capability of joining and breaking of these NWs following a flexible method that can work in diverse situations [8,9]. Furthermore, nanogaps produced by breaking NWs in a controlled manner can find applications in nanoelectronics [10], nanoplasmonics [11], and so on. In molecular electronics, the electrical transport or optical properties of one or more molecules bridging a nanogap can be measured, as the metal NWs can act like electrodes. The narrow space between two metal nanostructures can greatly enhance the local field due to the local surface plasmon resonances in nanoplasmonics. Therefore, a reliable and reproducible fabrication technique of nanogaps in metal NWs has become an active field of research.

So far, various methods such as focused ion beam [12,13], mechanical [14], chemical [15], templated electroplating [16,17], electromigration [18], and photothermal-induced [1] nanobreaking have been demonstrated for successfully fabricating nanogaps. Photothermal-induced nanobreaking provides many advantages over the other methods in terms of spatial position selection of nanobreaking, non-contact handling, and cost effectiveness. However, a gap width below 300 nm could not be realized following this method [1]. Furthermore, the field of photothermal-induced stress at nanoscale and fabrication of nanogap with controllably variable gap width starting from a few nm (<10 nm) by this method have not been explored yet.

In this Letter, an improvised photothermal-induced nanobreaking method utilizing a focused continuous-wave (CW) laser has been introduced for targeted breaking of Ag NWs in a controlled manner towards fabricating nanogaps with variable gap width starting from a few nm. The introduction of a metal thin film or a semiconductor NW under the metal NW causes localization of heat arising due to strong light absorption, which in turn generates a temperature gradient between the top and bottom (which is in contact with metal thin film/semiconductor NW) surfaces of the metal NW. The Rayleigh instability and photothermal-induced stress arising due to this temperature gradient along with melting/sublimation, which comes into play when the temperature is close to the melting point, aid in breaking the metal NW. A comprehensive comparative study to understand the role of different substrates in deciding the

resultant photothermal-induced stress and corresponding nanogap width (g) has been demonstrated. This ability to fabricate variable gap width starting from a few nm (<10 nm) can find application in molecular electronics.

Nanostructures consisting of noble metals, such as Ag and gold (Au), exhibit strong plasmon resonances when excited with light at visible frequencies. The excitation of resonant surface modes enhances the local electromagnetic field. These effects cause the intensification of light absorption. The absorption of light by the metal nanostructures, in turn, produces heat, which increases the temperature of the nanostructures. Thermal stress comes into the picture when a temperature gradient is developed, whereas melting/sublimation overtakes when the laser power is high enough to raise the temperature close to or above its melting point.

In this technique, a focused CW laser ($\lambda = 532$ nm) shot (duration $\tau = 4$ ms and beam waist ~400 nm) is used to break the Ag NWs placed on different substrates. To focus the laser beam, a microscope objective (100×) is used, and the sample is mounted on a 3D nanometer (least step size = 30 nm) scanning stage to break the NW accurately at the targeted point. The laser polarization and power are manipulated by using a combination of two polarizers and one half-wave plate. Ag NWs (synthesized by a self-seeding approach [19]) of different diameters (D) and of fixed length ($L \sim 10$ μm), and parallel polarization (i.e., the electric field is parallel to the long axis of the NW) of the laser beam have been used. The parallel polarization provides greater control over the breaking process compared to perpendicular polarization as the change in temperature due to change in power is more drastic in the case of perpendicular polarization [9].

Utilizing this photothermal effect, two different approaches have been demonstrated towards realizing fabrication of variable sub-100 nm gaps by breaking Ag NWs. In these approaches, different substrates (Au thin film, ZnO NW on silica, and bare silica) have been used (Fig. 1). It has been observed that Rayleigh instability plays a dominant role in breaking the Ag NW in the case of the Au thin film substrate, whereas photothermal-induced stress is mainly responsible in the case of the ZnO NW substrate. More details exploring the role of these substrates in determining g are provided in the subsequent sections.

Breaking of Ag nanowires placed on an Au thin film. Different incident laser powers are used to break the NWs of different diameters placed on an Au thin film (thickness = 100 nm) deposited on a silica substrate. The schematic diagram of the breaking process is shown in Fig. 1(a). Scanning electron microscopy (SEM) images of the broken Ag NWs placed on Au thin film are shown in Figs. 2(a)–2(h). The nanogap widths obtained from the SEM images vary from 20 nm to a few 100 nm corresponding to incident laser powers varying from 151 mW to 164 mW. A careful look at the SEM images reveals one interesting fact: the morphology of the broken NW shows undulation and the ends become much sharper compared to the initial diameter of the NW. It can also be observed that the critical minimum power (CMP) required for initializing the breaking of the NWs increases with diameter of the NWs, and also g increases with incident laser power [Fig. 2(i)].

Towards understanding the underlying physical mechanisms responsible for breaking of the Ag NWs, finite-difference time-domain (FDTD) and COMSOL simulations have been

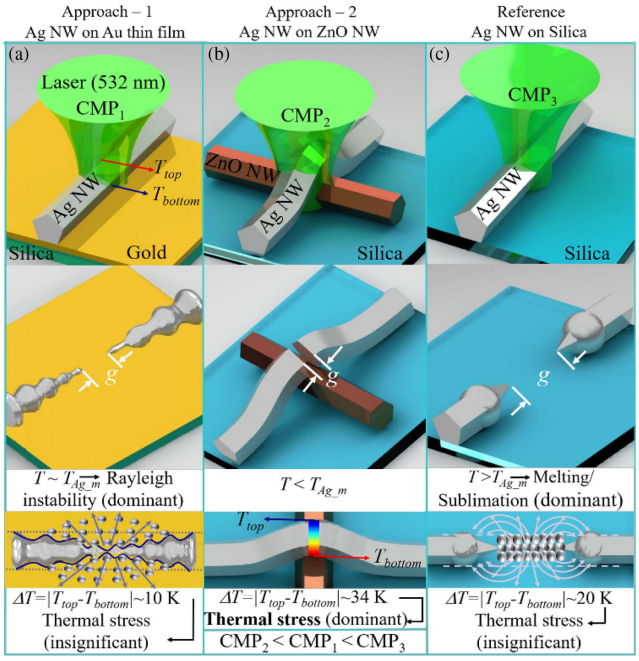

Fig. 1. Schematic diagrams depicting different approaches of breaking of Ag NWs using a focused CW laser when placed on (a) an Au thin film, (b) ZnO NWs, and (c) a silica substrate. T_{top} and T_{bottom} are the temperatures of the top and bottom surfaces of the Ag NW, respectively; T is the average temperature, and ΔTis the temperature difference between them. T_{Ag_m} represents the melting point of Ag. CMP is the required critical minimum power to initiate the breaking of the NW. The dotted lines indicate initial shape of the NWs.

performed, and the detailed simulation method can be found in Ref. [9]. A Gaussian laser source with beam waist dimeter of about 400 nm is considered for simulations. The high light absorption and thermal conductivity of the Au thin film play an important role in deciding the CMP, and thereby the gap width. From the simulation results, it has been observed that high light absorption helps in decreasing CMP (i.e., the temperature at which the NW breaks is reached at lower incident laser power), whereas high thermal conductivity has the reverse effect [Fig. 2(j)]. The nanogap width obtained for the incident laser power of 160 mW and the NW diameter of 300 nm is about 20 nm [Fig. 2(a)], and the corresponding simulated two-dimensional plot of temperature distribution shows that the maximum temperature at the focal point reaches 1205 K [Fig. 3(a)] which is close to T_{Ag_m}. The enhanced absorption of light owing to the excitation of surface plasmon modes, which is evident from the electric field distribution [Fig. 3(b)], raises the temperature of the NW at the focal point. This rise in temperature sublimates the Ag atoms around the focal point, which is evident from the thinner diameter at the breaking point compared to the initial diameter of the NW before laser exposure [Figs. 2(a)–2(h)]. It is observed from the simulated one-dimensional plot of temperature distribution that the temperature difference between the top and bottom surfaces of the Ag NW is 10 K [Fig. 3(c)]. The corresponding estimated thermal stress ($\sigma = Y \cdot \alpha \cdot \Delta T$, where $\alpha \sim 19 \times 10^{-6}$ K^{-1} [20] and $Y \sim 83$ GPa [21] are the linear thermal expansion coefficient and Young's modulus of Ag, respectively; ΔT is the

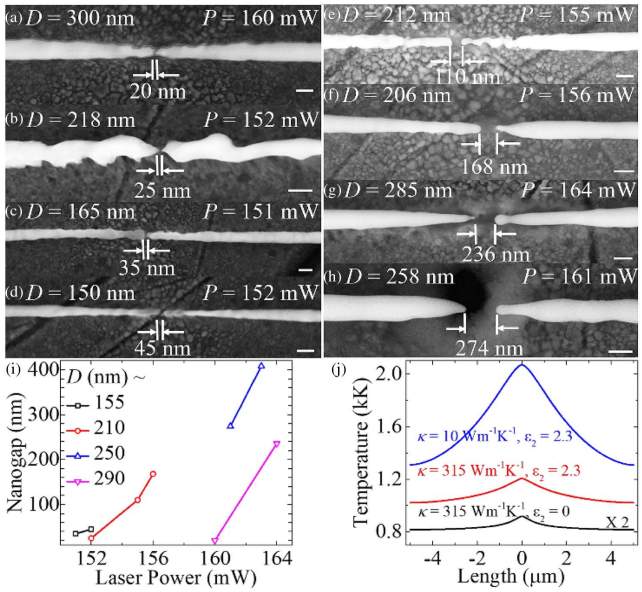

Fig. 2. SEM images of the broken Ag NWs placed on an Au thin film. (a)–(h) Images are arranged in ascending order of g. The scale bars are 200 nm. (i) Nanogap width versus incident laser power plot corresponding to NWs of different D. (j) Temperature distribution plot along the Ag NW considering zero absorption (fixed imaginary part of the relative permittivity ($\varepsilon = \varepsilon_1 + i\varepsilon_2$) to be zero, i.e., $\varepsilon_2 = 0$), significantly smaller thermal conductivity ($\kappa = 10$ Wm^{-1} K^{-1}), and actual values of relative permittivity ($\varepsilon_2 = 2.3$) and thermal conductivity ($\kappa = 315$ Wm^{-1} K^{-1}) of the Au thin film. The D and L of the Ag NW and the incident laser power are considered to be 300 nm, 10 μm, and 160 mW, respectively.

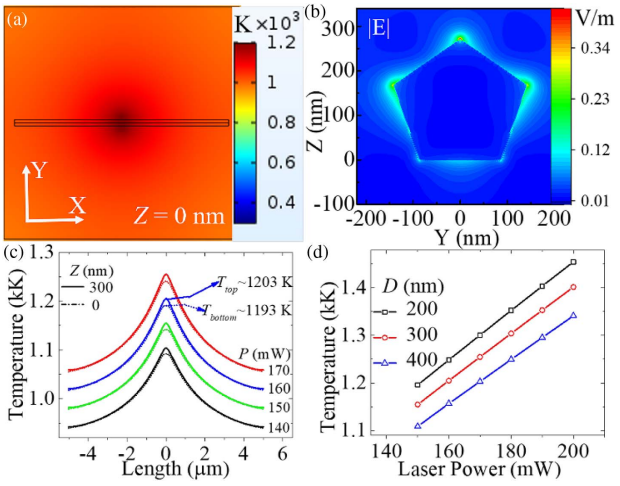

Fig. 3. Simulated results corresponding to the breaking of Ag NWs placed on an Au thin film. (a) 2D plot of temperature distribution for the incident laser power of 160 mW in the $Z = 0$ nm plane, i.e., top surface of the Au thin film. (b) Electric field distribution at the end of the Ag NW. (c) 1D plot of temperature distribution along the long axis of the Ag NW for different incident laser powers. The continuous and dashed lines represent the temperatures of the top and bottom surfaces of the Ag NW, respectively. For (a)–(c), the diameter and length of the NW are fixed at 300 nm and 10 μm, respectively. (d) Maximum temperature versus incident laser power plots for various diameters of NWs [fixed $L = 10$ μm and parallel polarization (E_x)].

temperature difference) comes out to be 16 MPa, which is on the same order as the elastic limit (~45 MPa) [22] of Ag at room temperature. However, the thermal stress can be neglected as the Ag NW is very ductile [8], and the temperature is close to its melting point. The breakup and undulation of NWs at near melting point temperature indicate that these NWs experience Rayleigh instability [23]. The simulated results obtained regarding the dependence of CMP on diameter of the Ag NW demonstrate that the required power increases with the NW diameter [Fig. 3(d)], which is also in agreement with the obtained experimental results [Fig. 2(i)].

Breaking of Ag nanowires placed on ZnO nanowires. In this section, we report the breaking of Ag NWs placed on ZnO NWs [Fig. 1(b)]. The experimental method is similar to the one described in the previous section. The replacement of Au thin film by ZnO NW changes the photophysical processes, specifically the absorption and heat conduction, and thereby changes the underlying physical mechanisms of breaking of Ag NWs.

The SEM images of the nanogaps obtained by controlled breaking of Ag NWs are shown in Fig. 4. The obtained g ranges from a few nm to a few hundred nm, corresponding to the incident laser power ranging from 94 mW to 100 mW. Surprisingly, the CMP is much lower in this case compared to the Au thin film substrate case, and therefore much lower g (<10 nm) could be obtained in this case [Figs. 4(c) and 4(d)]. The SEM images depicting the state of the Ag NWs for the incident power just below CMP are shown in Figs. 4(a) and 4(b).

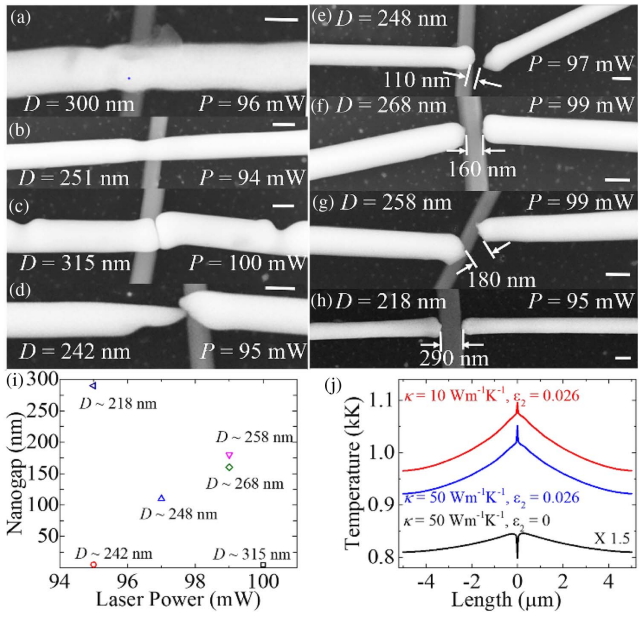

Fig. 4. SEM images of broken Ag NWs placed on ZnO NWs. The images are arranged (a)–(h) in ascending order of nanogap width. The scale bars are 200 nm for all images. (i) Nanogap width versus laser power plot corresponding to NWs of different diameters. The g under 10 nm could not be resolved from the SEM images, and is thereby represented by $g = 5$ nm. (j) Temperature distribution plot along the Ag NW considering zero absorption, significantly smaller thermal conductivity, and actual values of relative permittivity and thermal conductivity of the ZnO NW. The D and L of both Ag and ZnO NWs and the incident laser power are considered to be 300 nm, 10 μm, and 100 mW, respectively.

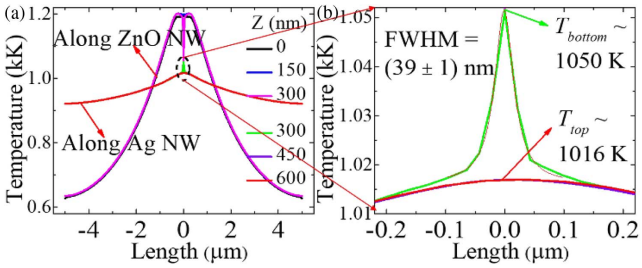

Fig. 5. (a) Simulated 1D plot of temperature distribution along the long axis of the NWs. The diameter and length of both the Ag and ZnO NWs and the incident laser power are considered to be 300 nm, 10 μm, and 100 mW, respectively. (b) Zoomed-in image of (a) showing ΔT between the top and bottom surfaces of the Ag NW placed on ZnO NW.

Careful inspection of the SEM images [Figs. 4(e)–4(h)] reveals a distinctive characteristic: the morphology of the broken ends of the Ag NW is flat, indicating little Rayleigh instability or melting or sublimation. The variation of g for different NWs corresponding to variable incident laser power is shown in Fig. 4(i). The light absorption and conductivity of ZnO have similar effect as in the case of Au thin film substrate [Figs. 2(j) and 4(j)].

To understand the reason for this peculiar behavior of low CMP value, we simulated the temperature distribution along the NWs. The 1D temperature distribution plots show that the maximum temperatures of the ZnO and Ag NWs are 1200 K and 1050 K, respectively [Fig. 5(a)]. These maximum temperatures are much lower than their respective melting points, and therefore none of the NWs (Ag and ZnO) melts. However, for the Ag NW, the temperature difference between the top and bottom surfaces at the breaking point is 34 K [Fig. 5(b)]. The corresponding thermal stress comes out to be about 54 MPa, which is larger than the elastic limit of Ag, and therefore the NW breaks even at this low temperature (lower than T_{Ag_m}). It can be noted that the temperature changes drastically along the long axis of the Ag NW as well [Fig. 5(b)], but this variation is for just the bottom surface of the Ag NW, and therefore it plays a limited role in the breaking of the NW. Therefore, it can be concluded that the NW breaks mainly due to photothermal-induced stress generated across the top and bottom surfaces of the NW at the breaking point. This is also evident from the SEM images showing flat cross sections of the broken NWs at the breaking point [Figs. 4(e)–4(h)], which show little evidence of melting/sublimation of Ag atoms, unlike in the case of the Au thin film substrate [Figs. 2(a)–2(h)]. Furthermore, the limited spread (full width at half-maximum, FWHM ~40 nm) of the temperature gradient along the length of the NW helps in achieving narrow gaps [Fig. 5(b)].

In the case of an Ag NW placed on silica substrate, the CMP is much higher (~280 mW for a NW with $D \sim 300$ nm and $L \sim 10$ μm) compared to that in the other two cases, and therefore the minimum g is also much larger [1].

In conclusion, an improvised photothermal-induced nanobreaking method utilizing a focused CW laser (532 nm) has been introduced for targeted breaking of Ag NW in a controlled manner to obtain variable gap width at sub-100 nm scale. Instead of silica substrate, when Au thin film or ZnO NW are introduced, the required CMP, which is a limiting factor to achieve narrower gaps, gets lowered drastically from about 280 mW (silica substrate) to about 160 mW (for Au thin film substrate) and 100 mW (for ZnO NW substrate) to break an Ag NW of diameter 300 nm and length 10 μm. Typically, it has been observed that Rayleigh instability plays a predominant role in breaking Ag NWs on Au thin film, whereas photothermal-induced stress and melting/sublimation are responsible for ZnO NW and silica substrates, respectively. The photothermal-induced stress corresponding to the CMP surpasses the elastic limit of the Ag NW and aids in breaking the NW; thereafter, nanogaps with variable gap width starting from a few nm (<10 nm) are fabricated by increasing the incident laser power above CMP. We demonstrate that this method is robust, and controlled nanogap width can be obtained for a wide range of NW sizes. This ability to fabricate variable gap width can find applications in molecular electronics.

Funding. National Key Research and Development Program of China (2017YFA0205700, 2017YFE0100200); National Natural Science Foundation of China (NSFC) (61425023, 61575177, 61775194).

REFERENCES

1. L. Zhou, J. Lu, H. Yang, S. Luo, W. Wang, J. Lv, M. Qiu, and Q. Li, Appl. Phys. Lett. **110**, 081101 (2017).
2. R. Yan, D. Gargas, and P. Yang, Nat. Photonics **3**, 569 (2009).
3. M. Singh, D. Movia, K. Mahfoud Omar, Y. Volkov, and A. Prina-Mello, Eur. J. Nanomed. **5**, 195 (2013).
4. J.-W. Chang, M. Jung, S. G. Kim, S.-B. Shim, J. Kim, S. G. Lee, Y. Yoo, and B. Kim, J. Korean Phys. Soc. **63**, 263 (2013).
5. K. Ellmer, Nat. Photonics **6**, 809 (2012).
6. L. Daniel, G. Gaël, M. Céline, C. Caroline, B. Daniel, and S. Jean-Pierre, Nanotechnology **24**, 452001 (2013).
7. Q. Nian, M. Saei, Y. Xu, G. Sabyasachi, B. Deng, Y. P. Chen, and G. J. Cheng, ACS Nano **9**, 10018 (2015).
8. L. Liu, D. Shen, G. Zou, P. Peng, and Y. Zhou, Scr. Mater. **114**, 112 (2016).
9. P. Ghosh, J. Lu, Z. Chen, H. Yang, M. Qiu, and Q. Li, Adv. Electron. Mater. **11**, 1700614 (2018).
10. P. Motto, A. Dimonte, I. Rattalino, D. Demarchi, G. Piccinini, and P. Civera, Nanoscale Res. Lett. **7**, 113 (2012).
11. W. Zhu, R. Esteban, A. G. Borisov, J. J. Baumberg, P. Nordlander, H. J. Lezec, J. Aizpurua, and K. B. Crozier, Nat. Commun. **7**, 11495 (2016).
12. A. Cui, Z. Liu, H. Dong, Y. Wang, Y. Zhen, W. Li, J. Li, C. Gu, and W. Hu, Adv. Mater. **27**, 3002 (2015).
13. A. Fursina, S. Lee, R. G. S. Sofin, I. V. Shvets, and D. Natelson, Appl. Phys. Lett. **92**, 113102 (2008).
14. S. Bertolazzi, J. Brivio, and A. Kis, ACS Nano **5**, 9703 (2011).
15. X. Chen, S. Yeganeh, L. Qin, S. Li, C. Xue, A. B. Braunschweig, G. C. Schatz, M. A. Ratner, and C. A. Mirkin, Nano Lett. **9**, 3974 (2009).
16. Y. Yasutake, K. Kono, M. Kanehara, T. Teranishi, M. R. Buitelaar, C. G. Smith, and Y. Majima, Appl. Phys. Lett. **91**, 203107 (2007).
17. V. M. Serdio V, T. Muraki, S. Takeshita, D. E. Hurtado, S. Kano, T. Teranishi, and Y. Majima, RSC Adv. **5**, 22160 (2015).
18. H. Park, A. K. L. Lim, A. P. Alivisatos, J. Park, and P. L. McEuen, Appl. Phys. Lett. **75**, 301 (1999).
19. S. Yugang and X. Younan, Adv. Mater. **14**, 833 (2002).
20. G. K. White and J. G. Collins, J. Low Temp. Phys. **7**, 43 (1972).
21. G. Y. Jing, H. L. Duan, X. M. Sun, Z. S. Zhang, J. Xu, Y. D. Li, J. X. Wang, and D. P. Yu, Phys. Rev. B **73**, 235409 (2006).
22. D. C. Ginnings, *Precision Measurement and Calibration: Heat* (U.S. Government Printing Office, 1970).
23. P. Peng, Z. Su, Z. Liu, Q. Yu, Z. Cheng, and J. Bao, Nanoscale **5**, 9532 (2013).